AIMS Mathematics, 8(7): 15932–15949.
DOI: 10.3934/math.2023813
Received: 17 February 2023
Revised: 21 March 2023
Accepted: 23 March 2023
Published: 04 May 2023

http://www.aimspress.com/journal/Math

Research article

Numerical investigation of non-transient comparative heat transport mechanism in ternary nanofluid under various physical constraints

Adnan[1,*], Waseem Abbas[1], Sayed M. Eldin[2] and Mutasem Z. Bani-Fwaz[3]

[1] Department of Mathematics, Mohi-ud-Din Islamic University, Nerian Sharif 12080, AJ&K, Pakistan
[2] Center of Research, Faculty of Engineering, Future University in Egypt, New Cairo 11835, Egypt
[3] Department of Chemistry, College of Science, King Khalid University, P.O. Box 9004, Abha 61413, Saudi Arabia

* **Correspondence:** Email: adnan_abbasi89@yahoo.com; Tel: +923315744284.

Abstract: *Significance:* The study of non-transient heat transport mechanism in mono nano as well as ternary nanofluids attracts the researchers because of their promising heat transport characteristics. Applications of these fluids spread in industrial and various engineering disciplines more specifically in chemical and applied thermal engineering. Due of huge significance of nanofluids, the study is organized for latest class termed as ternary nanofluids along with induced magnetic field.

Methodology: The model development done via similarity equations and the properties of ternary nanoparticles, resulting in a nonlinear mathematical model. To analyze the physical results with parametric values performed via RKF-45 scheme.

Study findings: The physical results of the model reveal that the velocity $F'(\eta)$ increased with increasing $m = 0.1, 0.2, 0.3$ and $\lambda_1 = 1.0, 1.2, 1.3$. However, velocity decreased with increasing δ_1. Tangential velocity $G'(\eta)$ reduces rapidly near the wedge surface and increased with increasing $M_1 = 1.0, 1.2, 1.3$. Further, the heat transport in ternary nanofluid was greater than in the hybrid and mono nanofluids. Shear drag and the local thermal gradient increased with increasing λ_1 and these quantities were greatest in the ternary nanofluid.

Keywords: ternary nanofluid; heat transfer; magnetic field; wedge; numerical analysis
Mathematics Subject Classification: 76-11, 76D05

Nomenclature

$\bar{u}, \bar{v}$	velocity along measure coordinates [m/s]
μ_{ternnf}	enhanced dynamic viscosity [Pa s]
μ_{hbnf}	enhanced bihybrid dynamic viscosity [Pa s]
ρ_{ternnf}	enhanced density [kg/m^3]
ρ_{hbnf}	enhanced bihybrid density [kg/m^3]
α_{ternnf}	enhanced thermal diffusivity [m^2/s]
k_{ternnf}	enhanced thermal conductivity [W/(m K)]
k_{hbnf}	enhanced bihybrid thermal conductivity [W/(m K)]
$\left(\rho c_p\right)_{ternnf}$	improved heat capacity [J/K]
$\left(\rho c_p\right)_{hbnf}$	improved bihybrid heat capacity [J/K]
$\bar{T}$	temperature [K]
$\bar{T}_\infty$	ambient temperature [K]
$\bar{T}_w$	wedge surface temperature [K]
$\bar{u}_w$	velocity at the surface [m/s]
$\bar{\omega}_1, \bar{\omega}_2, \bar{\omega}_3$	solid concentration of nanoparticles
M_1	magnetic number
P_r	Prandtl number
η	transformative variable
F'	dimensionless velocity
β	dimensionless temperature
λ_1	wedge parameter

1. Introduction

In the present time, promising characteristics of nanofluids and their hybrid types [1,2] attained much interest of the researchers and engineers. Thus, Kudenatti et al. [3] analyzed the dynamics of Power Law Nanofluid (PLN) over a non-static wedge. The authors emphasized on the importance of MHD and their role in the controlling motion of the fluid. Later on, Akcay et al. [4] reported the behaviour of shear drag along a moving wedge by engaging the multiple effects of the significant physical controlling parameters. Also, analysis of the velocity and temperature distribution over the surface was major focus of the authors. The study of non-transient heat transport playing key role in many of the applied research areas and change the fluid movement under the multiple parameter ranges Therefore, Jafar et al. [5] provided an in-depth analysis of steady magnetohydrodynamic [6] boundary layer flow and discussed variations in boundary layer region due to increasing values of the parameters.

The study of variety of nanoparticles with enhanced characteristics attracted the researchers and engineers. Therefore, extensive efforts have been made to investigate the nanofluids characteristics from various physical aspects. In 2013, Ellahi [7] discussed the potential effects of MHD on non-newtonian nanoliquid. The model developed using thermal dependent viscosity and the model solutions computed via analytical scheme and analyzed the dynamics of the model for multiple appeared parameters. Irreversibility analysis of power-law nanoliquid for electro osmotic CPF (Couette-Poiseuille flow)

reported in [8]. To improve the heat capability of the basic fluid, the authors preferred Al_2O_3 nanoparticles and examined interesting variations in entropy generation. In 2022, Bhatti et al. [9] emphasized on the study of magneto-nanoliquid using bihybrid nanoparticles. Diminishes in the fluid movement and concentration boundary layer with increasing magnetic, slip and Schmidt effects were core findings of the study. Besides these, nanoparticles extensively contribute in drug delivery systems. In this regard, a useful analysis provided by Bhatti et al. [10] and concluded that the study would be advantageous for biomedical engineering and those who are striving to investigate the dynamics of blood in arteries.

In 2023, Yasir et al. [11] performed thermal enhancement in bihybrid nanoliquids. The components of the working liquid taken as GO, Ag, AA7072 and MoS_2 and hybrid basic solvent H_2O/EG 50%/50%. The numerical simulation of the model done and analyzed the results of the interest and reported that the performed analysis would be expedient for electronic equipment cooling and heat exchangers devices. Abbas et al. [12] introduced a model for Sutterby nanofluid (SNF) by incorporating the influence of magnetic induction and Darcy resistance. The authors inspected that an increasing Eckert number corresponded to greater kinetic energy of the particles and thus an increase in temperature. Similarly, Murad et al. [13], Nisar et al. [14], Alsharari and Mousa [15] described deep knowledge about the characteristics of Casson-Carreau fluid directed to a stagnation point, changes in the nanoliquid performance due to slippery surface, activation energy, and buoyancy effects on copper/water nanofluid in the presence of an insulated obstacle. The studies showed that nanoliquids possessing outstanding thermal characteristics that ultimately increase their applications spectrum.

The transient heat transfer with hydrogen based nanoparticles and function fluid has tremendous characteristics and is extensively uses in multiple engineering disciplines. Thus, Mahmood and Khan [16] and Guedri et al. [17] analyzed the micropolar nanoliquid model and the effects of Al_2O_3 and Cu nanoparticles and on the heat transfer, shear drag and thermal transmission using basic fluid with hydrogen effects. The study supported findings that increasing the quantity of nanoparticles intensifies the shear drag coefficient and enhances the temperature of the fluid. Those researchers who are interesting in the field of nanofluids (see [18–22]) and their applications in various engineering zone paved their attention in the development of new innovative thermal transmission models and reported comparative or individual analysis. Some of the most latest and potential studies on various nanofluids described by the various scientists (for instance see [23–26]) using variety of tiny particles and basic functional fluid.

A comparative study of Sakiadis and Blasius flow reported by Klazly et al. [27]. The study revealed that shear drags rises for Sakiadis case and it drops for Blasius case. After that, Kumar et al. [28] reported MHD Blasius/Sakiadis flow of radiated Williamson fluid under effects of variable fluid characteristics. Devi et al. [29] focused on the investigation of 2D transient flow due to static sheet. Further, the authors integrated the significant effects of quadratic type radiation in chemically reactive fluid and interpreted the model results. The steady laminar boundary layer flow in the presence of Rosseland radiation was discussed by Pantokratoras et al. [30]. The study non-Newtonian Carreau, fluid along a static and a moving sheet reported in [31], examining wall shear drag and velocity profile for both Blasius and Sakiadis scenarios. Bataller [32] made efforts to analyze the surface convection effects on the boundary layer with thermal radiations effects. Hady et al. [33] discussed the heat transmission in single phase nanoliquids using shape factors effects. The effects of MHD and convective on BSF (Blasius and Sakiadis Flow) by using Cattaneo-Christov flux model over a sheet investigated in [34]. Similarly, the brief study of BSF using the effects of surface conditions and nanoparticles properties was reported by

Krishna et al. [35]. They concluded that the Nusselt number increases for Sakiadis flow. Further, the heat transport characteristics of BSF MHD Maxwell fluid was analyzed by Sekhar [36].

The study of electrically conducting non-Newtonian fluid under the variations of physical quantities investigated by Pantokratoras et al. [37]. The two-dimensional BSF flow of MHD radiated Williamson fluid with chemically reacting species of variable conductivity explored in [28]. The study of free convection for BSF through porous media investigated in [38]. Oyem et al. [39] performed the analysis of BSF of 2D incompressible fluid with soret/dufour effects. Pantokratoras et al. [40] discussed the BSF for Riga-surface and graphically analyzed the velocity profile as well as skin friction for both cases.

Heat transfer investigation in boundary layer flows attained huge attention of the researchers in all times. Such flows have potential applications in designing of airplane wings, nuclear thermal plants, aerodynamics, applied thermal engineering, chemical engineering and many other applied research areas. The researchers made efforts to analyze the heat transfer through boundary layer using simple, mono nano and bihybrid nanofluids under the influence of additional physical aspects. However, no attempt has be made to report the comparative thermal transmission under the influence of induced magnetic field in three types of nanofluids (mono nano, bihybrid and ternary nanofluids) which is important to discuss in the field. For this, reason the present study for boundary layer flow past a wedge (Falkner Skan flow) with pores at the surface is conducted. Modelling of the problem completed via transformative equations and new effective thermo physical characteristics of ternary nanofluids. The results of the model will be advantageous for various engineering applications where enhanced heat transfer is essential and the parametric ranges were considered for achieving better results.

2. Materials and methods

2.1. Model statement and physical configuration

Considered a steady incompressible and two-dimensional boundary layer flow through a wedge influenced by induced magnetic field. Let us supposed that, the velocities at the wedge surface and far from the wedge considered as $\bar{u}_w(x) = \bar{U}_w\, x^m$ and $\bar{u}_e(x) = \bar{U}_\infty\, x^m$, respectively. Here, $\bar{U}_w$, $\bar{U}_\infty$ are velocities and m is a constant with $0 \le m \le 1$. As Shown in Figure 1.

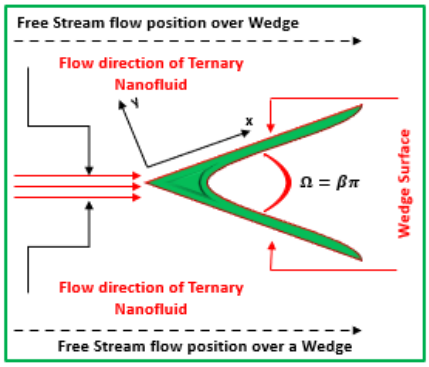

Figure 1. Physical flow scenario of ternary nanofluid past a wedge.

The governing equations according to the above considered model are as follows [41]:

$$\frac{\partial \bar{u}}{\partial x}+\frac{\partial \bar{v}}{\partial y}=0, \tag{1}$$

$$\frac{\partial \bar{H}_1}{\partial x}+\frac{\partial \bar{H}_2}{\partial y}=0, \tag{2}$$

$$\bar{u}\frac{\partial \bar{u}}{\partial x}+\bar{v}\frac{\partial \bar{u}}{\partial y}-\frac{\mu_{ternnf}}{4\pi\rho_f}\left(\bar{H}_1\frac{\partial \bar{H}_1}{\partial x}+\bar{H}_2\frac{\partial \bar{H}_1}{\partial y}\right)=\left(\bar{u}_e\frac{d\bar{u}_e}{dx}-\mu_{ternnf}\frac{\bar{H}_e}{4\pi\rho_f}\frac{d\bar{H}_e}{dx}\right)+\frac{\mu_{ternnf}}{\rho_{ternnf}}\frac{\partial^2\bar{u}}{\partial y^2}, \tag{3}$$

$$\bar{u}\frac{\partial \bar{H}_1}{\partial x}+\bar{v}\frac{\partial \bar{H}_1}{\partial y}-\bar{H}_1\frac{\partial \bar{u}}{\partial x}-\bar{H}_2\frac{\partial \bar{u}}{\partial y}=\mu_e\frac{\partial^2 H_1}{\partial y^2}, \tag{4}$$

$$\bar{u}\frac{\partial \bar{T}}{\partial x}+\bar{v}\frac{\partial \bar{T}}{\partial y}=\alpha_{ternf}\frac{\partial^2 \bar{T}}{\partial y^2}. \tag{5}$$

The applicable physical conditions for the current flow of ternary nanoliquid are considered as below:

$$\begin{cases}\bar{u}|_{y=0}=\bar{u}_w(x), \qquad \bar{v}|_{y=0}=0, \qquad \bar{T}|_{y=0}=\bar{T}_w,\\ \qquad\qquad \dfrac{\partial \bar{H}_1}{\partial y}|_{y=0}=\bar{H}_2|_{y=0}=0,\end{cases} \tag{6}$$

$$\begin{cases}\bar{u}\to\bar{u}_e(x)=\bar{U}_\infty x^m,\ \bar{T}\ \to\bar{T}_\infty,\\ \bar{H}_1|_{y\to\infty}=\bar{H}_e(x)=\bar{H}_0x^m.\end{cases} \text{ when } y\to\infty. \tag{7}$$

2.2. Nanofluids characteristics

Thermophysical properties of nanofluids [42,43] are of key interest in the analysis nanoliquids thermal transport. Therefore, the following properties (Table 1) of ternary nanofluid taken for estimation of enhanced nanoliquid characteristics.

Table 1. Equations for nanofluid, hybrid nanofluid and ternary nanofluid

Dynamic viscosity	
Nanofluid	$\mu_{nf}=\mu_f[1-\varpi_1]^{-2.5}$.
Hybrid nanofluid	$\mu_{hbnf}=\mu_f[(1-\varpi_1)^{2.5}(1-\varpi_2)^{2.5}]^{-1}$.
Ternary nanofluid	$\mu_{ternnf}=\mu_f[(1-\varpi_1)^{2.5}(1-\varpi_2)^{2.5}(1-\varpi_3)]^{-1}$.

Continued on next page

Density	
Nanofluid	$\rho_{nf} = \left[(1-\varpi_1) + \varpi_1 \frac{\rho_{p1}}{\rho_f}\right]\rho_f.$
Hybrid nanofluid	$\rho_{hbnf} = (1-\varpi_2)\left[(1-\varpi_1) + \varpi_1 \frac{\rho_{p1}}{\rho_f}\right] + \varpi_2 \frac{\rho_{p2}}{\rho_f}.$
Ternary nanofluid	$\rho_{ternf} = (1-\varpi_3)\left[\left\{(1-\varpi_2)\left[(1-\varpi_1) + \varpi_1 \frac{\rho_{p1}}{\rho_f}\right] + \varpi_2 \frac{\rho_{p2}}{\rho_f}\right\}\right] + \varpi_3 \frac{\rho_{p3}}{\rho_f}.$
Heat capacity	
Nanofluid	$(\rho c_p)_{nf} = \left[(1-\varpi_1) + \varpi_1 \frac{(\rho c_p)_{p1}}{(\rho c_p)_f}\right](\rho c_p)_f.$
Hybrid nanofluid	$(\rho c_p)_{hbnf} = (1-\varpi_2)\left[(1-\varpi_1) + \varpi_1 \frac{(\rho c_p)_{p1}}{(\rho c_p)_f}\right] + \varpi_2 \frac{(\rho c_p)_{p2}}{(\rho c_p)_f}.$
Ternary nanofluid	$(\rho c_p)_{ternf} = (1-\varpi_3)\left[\left\{(1-\varpi_2)\left[(1-\varpi_1) + \varpi_1 \frac{(\rho c_p)_{p1}}{(\rho c_p)_f}\right] + \varpi_2 \frac{(\rho c_p)_{p2}}{(\rho c_p)_f}\right\}\right] + \varpi_3 \frac{(\rho c_p)_{p3}}{(\rho c_p)_f}.$
Thermal conductivity	
Nanofluid	$k_{nf} = \frac{\left[(k_{p1}+2k_f) - 2\varpi_1(k_f - k_{p1})\right]}{\left[(k_{p1}+2k_f) + \varpi_1(k_f - k_{p1})\right]} k_f.$
Hybrid nanofluid	$k_{hbnf} = \frac{\left[(k_{p2}+2k_{nf}) - 2\varpi_2(k_{nf} - k_{p2})\right]}{\left[(k_{p2}+2k_{nf}) + \varpi_2(k_{nf} - k_{p2})\right]} k_{nf}.$
Ternary nanofluid	$k_{ternnf} = \frac{\left[(k_{p3}+2k_{hbnf}) - 2\varpi_3(k_{hbnf} - k_{p3})\right]}{\left[(k_{p3}+2k_{hbnf}) + \varpi_3(k_{hbnf} - k_{p3})\right]} k_{hbnf}.$

To acquire to desired heat transfer model, the following similarity equations were used along with mathematical operations:

$$\left.\begin{aligned} \overline{u} = \frac{\partial \overline{\psi}}{\partial y} = \bar{\mathrm{U}}_\infty x^m F^{'}, \overline{v} = -\frac{\partial \overline{\psi}}{\partial x} = -\left(\frac{(\overline{m}+1)\nu_f \overline{U}(x)}{2x}\right)^{\frac{1}{2}}\left(F + \frac{\overline{m}-1}{\overline{m}+1}\right)\eta F^{'}, \\ \overline{\psi} = \left(\frac{2\nu_f x U(x)}{(m+1)}\right)^{0.5} F, \beta = \frac{\overline{T}-\overline{T}_\infty}{\overline{T}_w - \overline{T}_\infty}, \eta = \left(\frac{(m+1)U(x)}{2\nu_f x}\right)^{0.5}, \\ \overline{H}_1 = \overline{H}_0 x^m G^{'}, \qquad \overline{H}_2 = -\overline{H}_o\left(\frac{2\nu_f x^{\overline{m}-1}}{(\overline{m}+1)\overline{U}_\infty}\right)^{0.5}\{\overline{m}G + 0.5(\overline{m}-1)\eta G^{'}\}. \end{aligned}\right\} \tag{8}$$

Finally, the following heat transport model obtained which includes the characteristics of ternary nanofluid.

$$F''' + \frac{\frac{\rho_{ternnf}}{\rho_f}}{\frac{\mu_{ternnf}}{\mu_f}}\left[F''F + 2m(m+1)^{-1}(1-F'^2) + \frac{2\delta_1}{(m+1)}(mG'^2 - mG''G - m)\right] = 0, \tag{9}$$

$$M_1 G''' + G''F - 2m(m+1)^{-1}F''G = 0, \tag{10}$$

$$\frac{k_{ternnf}}{k_f}\beta'' + \frac{Pr(\rho c_p)_{ternnf}}{(\rho c_p)_f}\beta' F = 0, \tag{11}$$

$$\frac{k_{ternnf}}{k_f} = \left[\frac{\left(k_{p1} + 2k_f\right) - 2\varpi_1\left(k_f - k_{p1}\right)}{\left(k_{p1} + 2k_f\right) + \varpi_1\left(k_f - k_{p1}\right)} * \frac{\left(k_{p2} + 2k_{nf}\right) - 2\varpi_2\left(k_{nf} - k_{p2}\right)}{\left(k_{p2} + 2k_{nf}\right) + \varpi_2\left(k_{nf} - k_{p2}\right)} * \frac{\left(k_{p3} + 2k_{hbnf}\right) - 2\varpi_3\left(k_{hbnf} - k_{p3}\right)}{\left(k_{p3} + 2k_{hbnf}\right) + \varpi_3(k_{hbnf} - k_{p3})}\right].$$

The above-described model is supported by the following boundary conditions over the wedge:

$$F = 0, F' = \lambda_1, G = 0, G'' = 0, \beta = 1 \; at \; \eta = 0, \tag{12}$$

$$F' = 1, G = 1, \beta \to 0 \; when \; \eta \to \infty. \tag{13}$$

The embedded quantities are $\delta_1 = \frac{\bar{\mu}_e \bar{H}_0{}^2}{4\pi\rho_f \, \bar{U}_\infty{}^2}$, $Pr = \nu_f \alpha_f^{-1}$ and $\lambda_1 = \frac{\bar{U}_w}{\bar{U}_\infty}$. Moreover, the significant (skin friction and Nusselt number) formulas described by the following expressions (Table 2):

Table 2. Skin friction and Nusselt number expressions for nano, hybrid and ternary nanofluids.

Skin friction formulas	
Nanofluid	$\frac{[1-\varpi_1]^{-2.5}}{\left[(1-\varpi_1) + \varpi_1 \frac{\rho_{p1}}{\rho_f}\right]} F''(0).$
Hybrid nanofluid	$\frac{[(1-\varpi_1)^{2.5}(1-\varpi_2)^{2.5}]^{-1}}{(1-\varpi_2)\left[(1-\varpi_1) + \varpi_1 \frac{\rho_{p1}}{\rho_f}\right] + \varpi_2 \frac{\rho_{p2}}{\rho_f}} F''(0).$
Ternary nanofluid	$\frac{[(1-\varpi_1)^{2.5}(1-\varpi_2)^{2.5}(1-\varpi_3)]^{-1}}{(1-\varpi_3)\left[\left\{(1-\varpi_2)\left[(1-\varpi_1) + \varpi_1 \frac{\rho_{p1}}{\rho_f}\right] + \varpi_2 \frac{\rho_{p2}}{\rho_f}\right\}\right] + \varpi_3 \frac{\rho_{p3}}{\rho_f}} F''(0).$

Continued on next page

Nusselt number formulas	
Nanofluid	$\left\|\left[\frac{(k_{p1}+2k_f)-2\varpi_1(k_f-k_{p1})}{(k_{p1}+2k_f)+\varpi_1(k_f-k_{p1})}\right]\beta'(0)\right\|.$
Hybrid nanofluid	$\left\|\left[\frac{(k_{p1}+2k_f)-2\varpi_1(k_f-k_{p1})}{(k_{p1}+2k_f)+\varpi_1(k_f-k_{p1})}*\frac{(k_{p2}+2k_{nf})-2\varpi_2(k_{nf}-k_{p2})}{(k_{p2}+2k_{nf})+\varpi_2(k_{nf}-k_{p2})}\right]\beta'(0)\right\|.$
Ternary nanofluid	$\left\|\left[\begin{matrix}\frac{(k_{p1}+2k_f)-2\varpi_1(k_f-k_{p1})}{(k_{p1}+2k_f)+\varpi_1(k_f-k_{p1})}*\frac{(k_{p2}+2k_{nf})-2\varpi_2(k_{nf}-k_{p2})}{(k_{p2}+2k_{nf})+\varpi_2(k_{nf}-k_{p2})}* \\ \frac{(k_{p3}+2k_{hbnf})-2\varpi_3(k_{hbnf}-k_{p3})}{(k_{p3}+2k_{hbnf})+\varpi_3(k_{hbnf}-k_{p3})}\end{matrix}\right]\beta'(0)\right\|.$

2.3. Mathematical analysis

The current model is coupled and contains high nonlinearities, and an exact solution is not feasible. Therefore, the RKF-45 (see [44–46]) implemented for the analysis of the model using the software MATHEMATICA 13.0 and the impacts of physical constraints on the heat transport performances of mono, hybrid and ternary nanofluids. The adopted technique is applicable for initial value problems and the desired initial value problem was obtained after using the following transforms in the system:

$$[\zeta_1,\zeta_2,\zeta_3,\zeta_3',\zeta_4,\zeta_5,\zeta_6,\zeta_6',\zeta_7,\zeta_8,\zeta_8'] = [F,F',F'',F''',G,G',G'',G''',\beta,\beta',\beta'']. \tag{14}$$

The system was then arranged in the following way to reduce it into respective initial value problems.

$$F''' = -\frac{\frac{\rho_{ternnf}}{\rho_f}}{\frac{\mu_{ternnf}}{\mu_f}}\left[F''F+2m(m+1)^{-1}(1-F'^2)+\frac{2\delta_1}{(m+1)}(mG'^2-mG''G-m)\right], \tag{15}$$

$$G''' = -\frac{1}{M_1}[G''F-2m(m+1)^{-1}F''G], \tag{16}$$

$$\beta'' = -\frac{1}{\frac{k_{ternnf}}{k_f}}\left[\frac{Pr(\rho c_p)_{ternnf}}{(\rho c_p)_f}\beta'F\right]. \tag{17}$$

Now, the system takes the below appropriate form for further computation:

$$\zeta_3' = -\frac{\frac{\rho_{ternnf}}{\rho_f}}{\frac{\mu_{ternnf}}{\mu_f}}\left[\zeta_3\zeta_1+2m(m+1)^{-1}(1-\zeta_2^2)+\frac{2\delta_1}{(m+1)}(m\zeta_5^2-m\zeta_5'\zeta_4-m)\right], \tag{18}$$

$$\zeta_6' = -\frac{1}{M_1}[\zeta_6\zeta_1-2m(m+1)^{-1}\zeta_3\zeta_4], \tag{19}$$

$$\zeta_8' = -\frac{1}{\frac{k_{ternnf}}{k_f}}\left[\frac{Pr\left(\rho c_p\right)_{ternnf}}{\left(\rho c_p\right)_f}\zeta_8\zeta_1\right]. \tag{20}$$

Accuracy of the technique is achieved by setting its tolerance up to 10^{-6} and the step size 0.01. The authenticity of the results is subject to the asymptotic behavior of the temperature profile and it must satisfy the boundary conditions for the velocity and temperature distributions. These are obvious from the plotted results which gives the correctness of the model results.

3. Results and discussion

The physical results of the model representing the flow of ternary, nano and bihybrid nanoliquids over a nonstationary wedge are demonstrated in this section. It is commendable to mention here that the three types of nanoparticles namely Al_2O_3, Cu and Ag taken for the formation of resultant nanoliquid and H_2O is taken as working base solvent due its good solvent characteristics, density and high heat capacity. Further, ϖ_1, ϖ_2 and ϖ_3 are the associated concentration of the nanoparticles in the basic solvent. Further, the concentrations of nanoparticles were taken up to 20% and feasible value of Prandtl number for water is fixed at 6.2. This section further classified into three subsequent subsections which represent the model results for the velocity, ternary nanoliquid temperature, shear drag and Nusselt number. The study validation is also presented in subsection 4.4.

3.1. Impacts of the flow parameters on $F'(\eta)$ and $G'(\eta)$

Figure 2 demonstrating the velocity $F'(\eta)$ changes under potential effects of m, moving wedge number λ_1 and magnetic number δ_1. The presentation of the velocity distribution shows that the fluid movement increases by enlarging the values of m and λ_1. Physically, when the wedge moves then the neighboring fluid layer on the wedge surface gain the velocity of the wedge. As a consequence the particles moves rapidly. Then the frictional forces with the successive fluid layer reduces and the fluid velocity increases. After, $\eta = 3.0$ the velocity of the fluid reaches to its maximum speed and then moves with the speed of free stream. These results elucidated in Figures 2(a) and 2(b), respectively. On the other side, the magnetic number reduces the fluid motion and almost negligible variations observed in Figure 2(c).

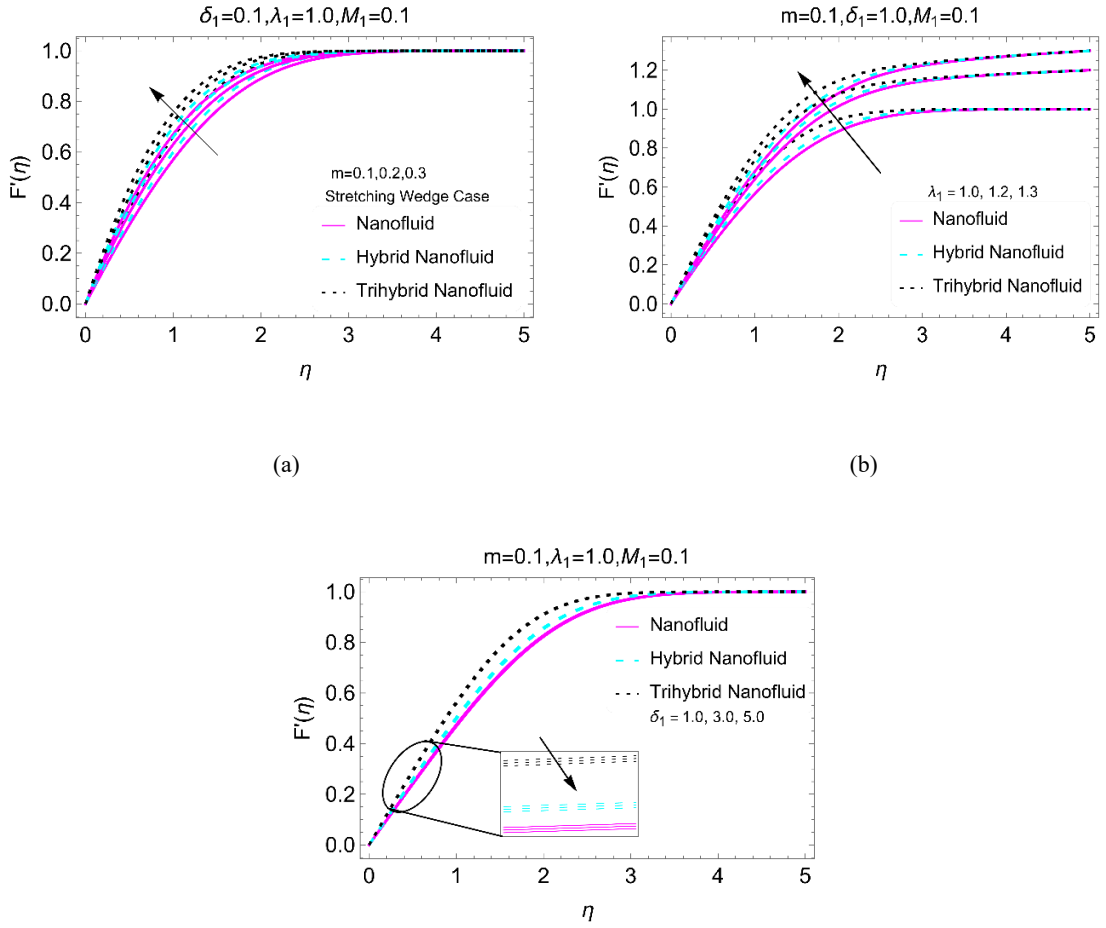

Figure 2. The velocity profile F' against different values of parameters (a) m,(b) λ_1, and (c)δ_1.

Figures 3 and 4 organized to analyze the tangential velocity distribution $G'(\eta)$ for increasing λ_1, M_1 and δ_1. The tangential velocity of the fluid varies in very interesting way while the wedge moves and the reciprocal Hartmann parameter M_1 enlarges. It is inspected that $G'(\eta)$ declines prominently near the wedge surface (Figure 3a); however, these variations become slow and finally reaches to the its maximum limit i.e., $G'(\eta) = 1$ after which the fluid moves with constant velocity. Figure 3(b) indicates that the reciprocal Hartmann parameter (Figure 3b) is effective in increasing the velocity component $G'(\eta)$ and is maximum fluctuation is observed around $\eta = 0$. The 3D representation of the results in Figures 3(a) and 3(b) given in Figures 3(c) and 3(d), respectively. Figure 4 demonstrating the impacts of δ_1 which shows that the velocity drops when the parameter δ_1 enhances and maximum drop is noticed for nanoliquids. Figure 4(d) supports the 3D pictorial view of the δ_1 variations on the profile of $G'(\eta)$.

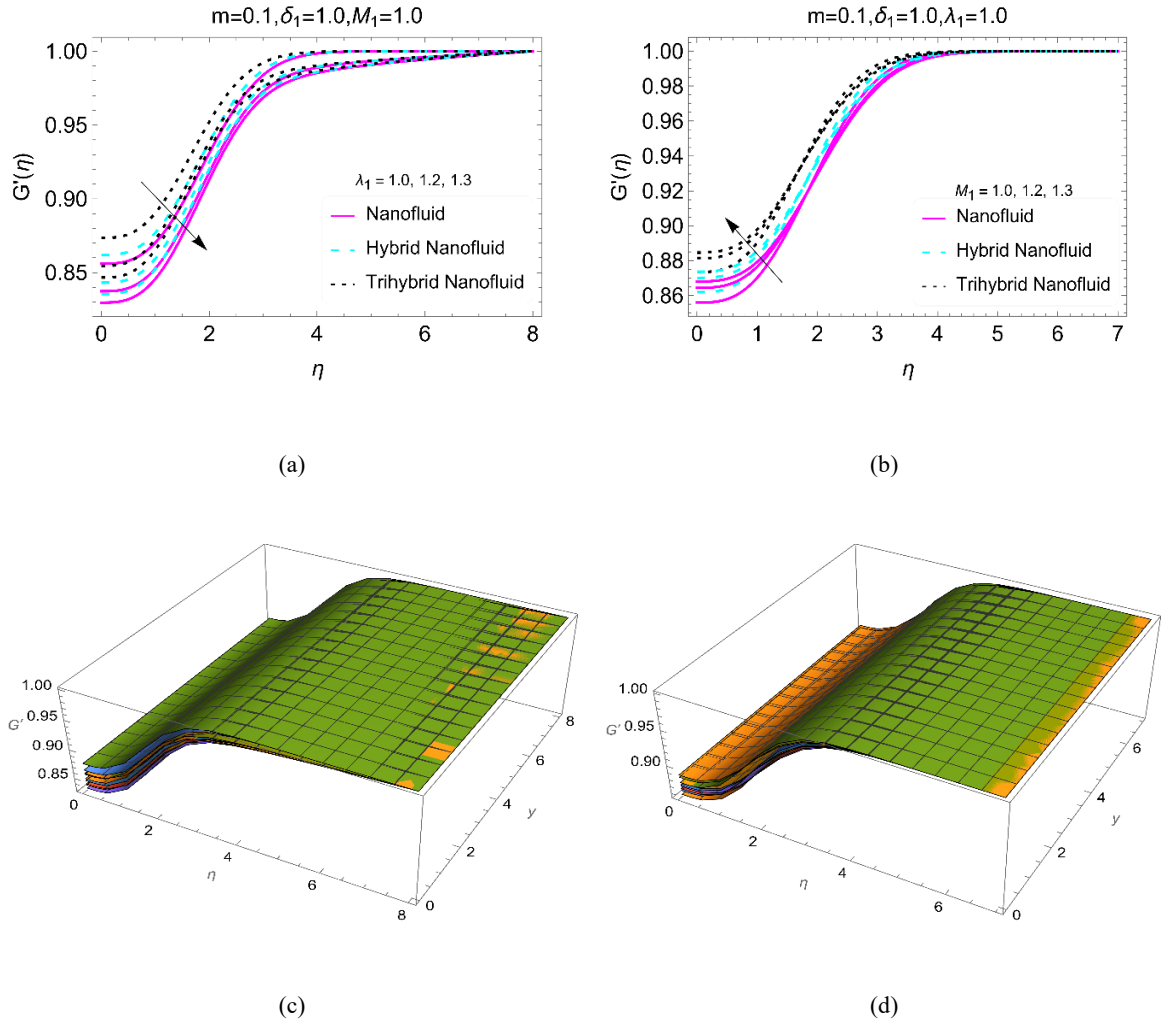

Figure 3. The velocity profile G′ against (a), (c) λ_1 and (b), (d) M_1.

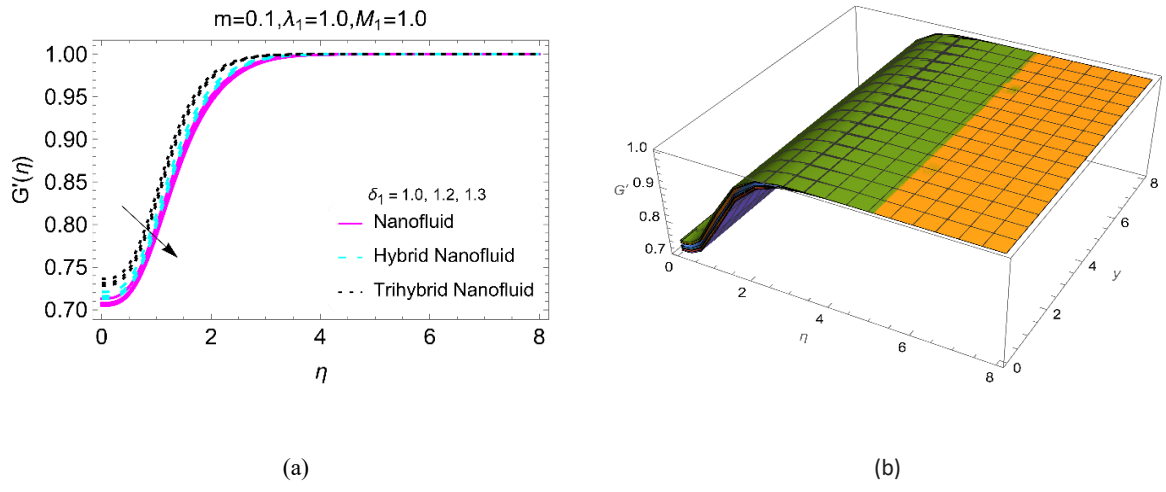

Figure 4. The velocity profile G’ against δ_1.

3.2. *Impacts of the flow parameters on temperature*

This subsection represents the comparative enhanced heat transfer for Al_2O_3/H_2O (mono nanoliquid), $(Al_2O_3\text{-}CuO)/H_2O$ (bihybrid nanoliquid) and $(Al_2O_3\text{-}CuO\text{-}Ag)/H_2O$ (ternary nanoliquid) due to variations in δ_1, λ_1 and M_1. For this, Figure 5 furnished.

Figure 5(a) indicates that when the magnetic forces enlarges, the temperature of the fluids also increases. However, higher temperatures are observed for ternary nanoliquid than bihybrid and mono nanoliquids. Physically, ternary nanoliquid $(Al_2O_3\text{-}CuO\text{-}Ag)/H_2O$ comprises the thermal conductivity and heat capacity of three particles which increase thermal conductivity of ternary nanoliquid which enhance it heat transport property. Thus, in ternary nanoliquid the heat transfer is greater than in the other nanofluids. Similarly, the temperature decreases with increasing λ_1 (Figure 5b) but the behavior is greater in the ternary nanofluid. Further, thermal boundary layer thickness increase for larger δ_1 and no significant contribution of the reciprocal Hartmann number (Figure 5c) was noticed in thermal enhancement of the nanofluids.

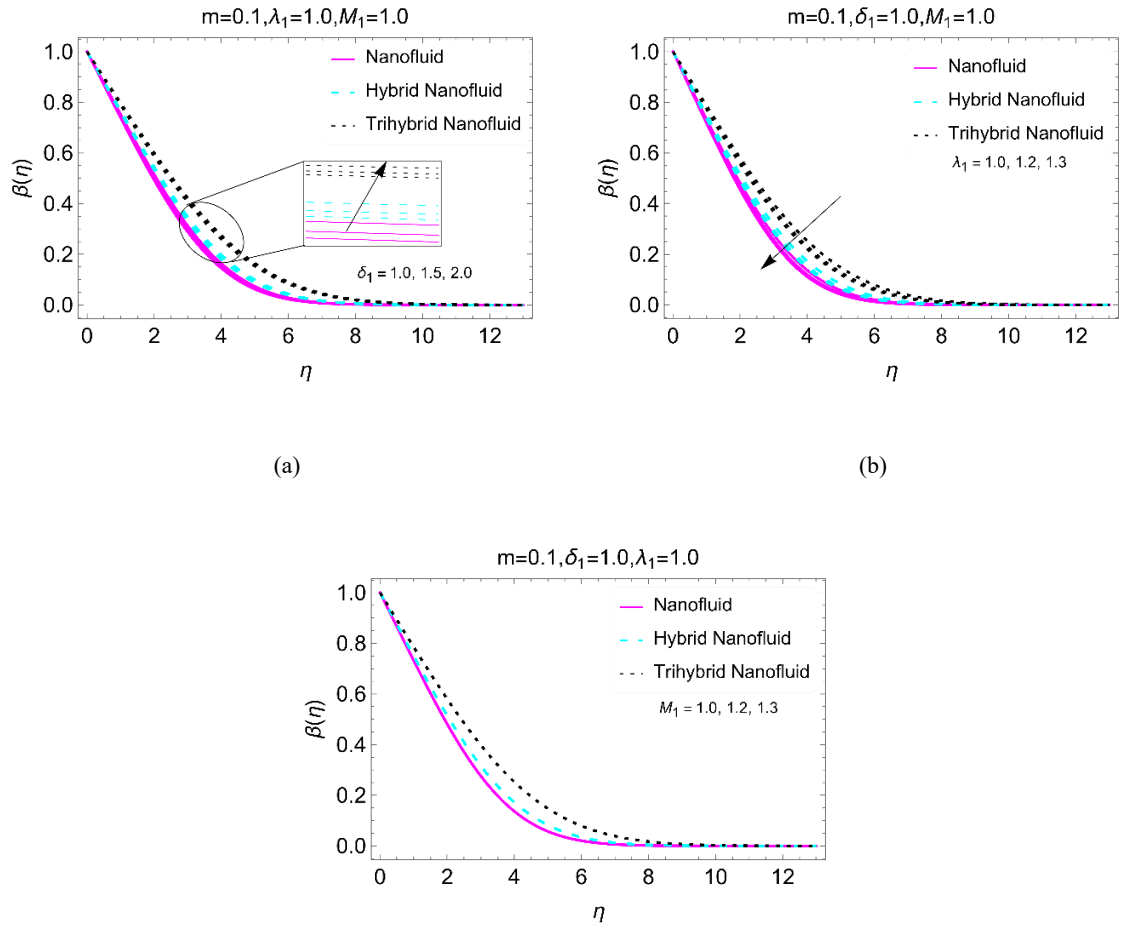

Figure 5. The temperature trends via (a) δ_1 (b) λ_1 and (c) M_1.

3.3. *Impacts of the flow parameters on shear drag and Nusselt number*

The study of shear drags and thermal gradient (Nusselt number) in nanofluids is essential from various engineering field and industrial purposes. Therefore, this subsection fill this requirement under the variations of the model parameters. For this, Figures 5 and 6 plotted for the shear drags and Nu trends.

Figures 6(a) and 6(b) present the shear drag in the mono nanofluid, bihybrid nanofluid and ternary nanofluid against δ_1 and λ_1, respectively. In both the cases, the greatest shear drag effects were in the ternary nanoliquids. Physically, composite density of (Al_2O_3-CuO-Ag) nanoparticles make the resultant fluid denser than that of mono (Al_2O_3) and bihybrid (Al_2O_3-CuO) nanoparticles. Due to this reason maximum shear drag observed on the wedge surface.

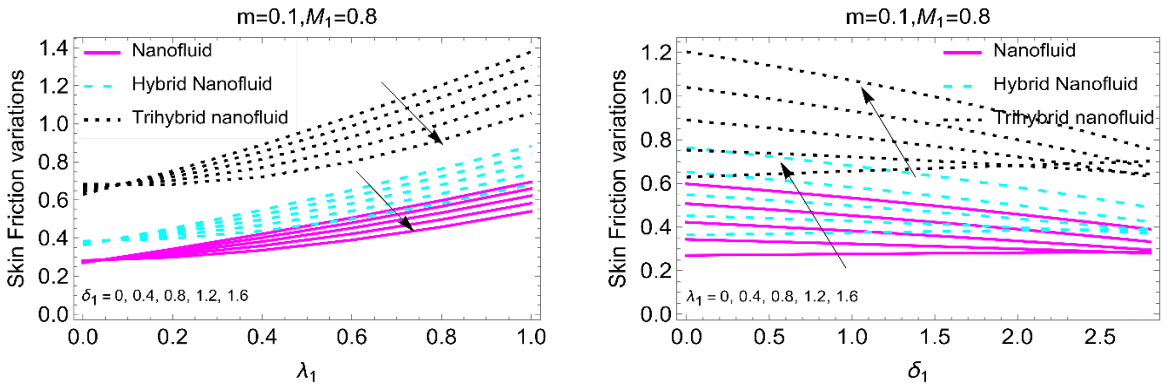

(a) (b)

Figure 6. The changes of skin friction against (a) δ_1 and (b) λ_1.

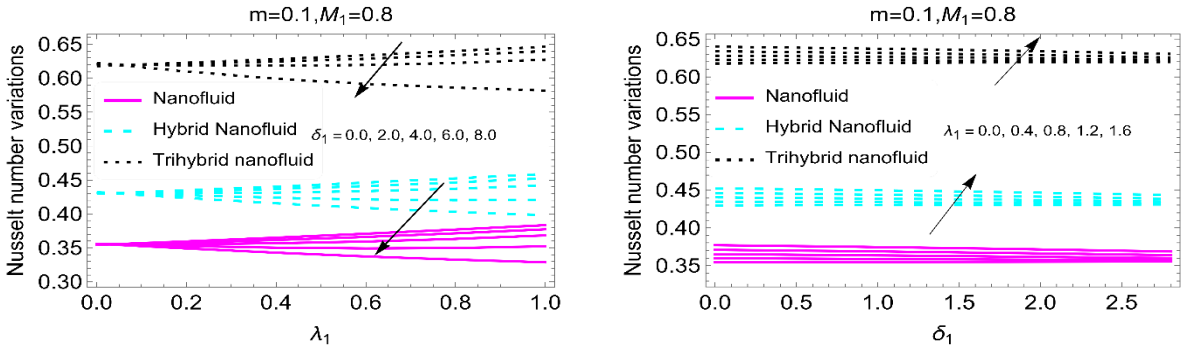

(a) (b)

Figure 7. The changes of Nu with increasing (a) $\delta_1$and (b) λ_1.

The analysis of thermal gradient at the surface is important for heating/cooling purposes. Thus, the set of Figures 7(a) and 7(b) show the trends of Nusselt number on the surface for increasing values of δ_1 and λ_1, respectively. For both parametric variations, the Nusselt number is greatest in the ternary

nanoliquid. Physically, the sum of thermal conductivities of the nanoparticles boosts the thermal conductivity of ternary nanofluid. Therefore, maximum heat transmitted on the wedge surface. However, for bihybrid and mono nanoliquids, the heat transport mechanism is slow due to weak thermal conductivity.

3.4. Study validation

The study validation successfully performed and is presented in this subsection. In order make the current model compatible with the existing models in open science literature, it is essential to set the values ϕ_j for $j = 1,2,3$, λ_1 and δ_1 such that these tends to zero. Then, the model results for shear drag $F''(0)$ computed at multiple stages of the parameter m. These results given in Table 3 and it is cleared that the current results aligned with the results of Ahmed et al. [47], Watanabe [48] and Adnan et al. [49]. This shows that the results obtained from the study are correct and can be replicated in future studies.

Table 3. Validation of the present model results with the previous efforts made by different researchers.

$\boldsymbol{m}$	Results from various studies for $\boldsymbol{F''(0)}$			
	present results	Ahmed et al. [47]	Watanabe [48]	Adnan et al. [49]
0.0	0.4695999960	0.46959	0.46960	0.469590
0.0141	0.5046143299	0.504614	-----	0.504614
0.0435	0.5689777817	0.568977	0.56898	0.568977
0.0909	0.6549788596	0.654978	0.65498	0.654978
0.1429	0.7319985706	0.731998	0.73200	0.731998
0.2000	0.8021256343	0.802125	0.80213	0.802125
0.3333	0.9276536249	0.927653	0.92765	0.927653
0.5000	1.0389035229	1.038903	1.03890	1.038903

4. Conclusions

The study of thermal enhancement in ternary nanofluids over a moving wedge amid an induced magnetic field is presented. The basic model was transformed into a simplified form via defined transformative rules and improved properties of the ternary nanofluid. To investigate the influence of the model parameters on the dynamics of fluid, numerical analysis was conducted and the results were portrayed multiple parametric values. It is concluded that:

- The fluids movement (nanofluid, hybrid nanofluid and ternary nanofluid) can be intensified by increasing the values of m and λ_1 as $0.1, 0.2, 0.3$ and $1.0, 1.2, 1.3$, respectively.
- The magnetic field strongly opposed the fluid velocity over the wedge surface.
- The tangential velocity $G'(\eta)$ diminishes rapidly when λ_1 and δ_1 increase as $1.0, 1.2, 1.3$.
- The ternary nanofluid has high capacity to transmit the heat with increasing δ_1, while the transmission in the nanofluid and hybrid nanoliquid is slow.
- The thermal gradient in ternary nanoliquid was 65%, for the hybrid nanofluid, it was 45% and for the common nanofluid it was 35% which shows that ternary nanofluids are excellent for thermal transport applications.

Acknowledgments

The authors extend their appreciation to the Deanship of Scientific Research at King Khalid University for funding this work through large group Research Project under grant number RGP2/16/44.

Conflict of interest

The authors declare no conflict of interest.

References

1. N. A. Shah, A. Wakif, E. R. El-Zahar, S. Ahmad, S. J. Yook, Numerical simulation of a thermally enhanced EMHD flow of a heterogeneous micropolar mixture comprising (60%)-Ethylene Glycol (EG), (40%)-water (W), and copper oxide nanomaterials (CuO), *Case Stud. Therm. Eng.*, **35** (2022), 102046. http://dx.doi.org/10.1016/j.csite.2022.102046
2. Adnan, K. A. M. Alharbi, M. Z. Bani-Fwaz, S. M. Eldin, M. F. Yassen, Numerical heat performance of TiO_2/Glycerin under nanoparticles aggregation and nonlinear radiative heat flux in dilating/squeezing channel, *Case Stud. Therm. Eng.*, **41** (2023), 102568. http://dx.doi.org/10.1016/j.csite.2022.102568
3. R. B. Kudenatti, N. E. Misbah, Hydrodynamic flow of non-Newtonian power-law fluid past a moving wedge or a stretching sheet: A unified computational approach, *Sci. Rep.*, **10** (2020), 9445. http://dx.doi.org/10.1038/s41598-020-66106-6
4. M. Akçay, M. A. Yükselen, Flow of power-law fluids over a moving wedge surface with wall mass injection, *Arch. Appl. Mech.*, **81** (2011), 65–76. http://dx.doi.org/10.1007/s00419-009-0393-z
5. K. Jafar, R. Nazar, A. Ishak, I. Pop, MHD boundary layer flow due to a moving wedge in a parallel stream with the induced magnetic field, *Bound. Value Probl.*, **2013** (2013), 20. http://dx.doi.org/10.1186/1687-2770-2013-20
6. Q. H. Shi, A. Hamid, M. I. Khan, R. N. Kumar, R. J. P. Gowda, B. C. Prasannakumara, et al., Numerical study of bio-convection flow of magneto-cross nanofluid containing gyrotactic microorganisms with activation energy, *Sci. Rep.*, **11** (2021), 16030. http://dx.doi.org/10.1038/s41598-021-95587-2
7. R. Ellahi, The effects of MHD and temperature dependent viscosity on the flow of non-Newtonian nanofluid in a pipe: Analytical solutions, *Appl. Math. Model.*, **37** (2013), 1451–1467. http://dx.doi.org/10.1016/j.apm.2012.04.004
8. R. Ellahi, S. M. Sait, N. Shehzad, N. Mobin, Numerical simulation and mathematical modeling of electro-osmotic Couette-Poiseuille flow of MHD power-law nanofluid with entropy generation, *Symmetry*, **11** (2019), 1038. http://dx.doi.org/10.3390/sym11081038
9. M. M. Bhatti, H. F. Öztop, R. Ellahi, Study of the magnetized hybrid nanofluid flow through a flat elastic surface with applications in solar energy, *Materials*, **15** (2022), 7507. http://dx.doi.org/10.3390/ma15217507
10. M. M. Bhatti, S. M. Sait, R. Ellahi, Magnetic nanoparticles for drug delivery through tapered stenosed artery with blood based non-Newtonian fluid, *Pharmaceuticals*, **15** (2022), 1352. http://dx.doi.org/10.3390/ph15111352

11. Y. Khan, S. Abdal, S. Hussain, I. Siddique, Numerical simulation for thermal enhancement of H_2O+Ethyl Glycol base hybrid nanofluid comprising GO+(Ag, AA7072, MoS2), *AIMS Math.*, **8** (2023), 11221–11237. http://dx.doi.org/10.3934/math.2023568
12. N. Abbas, W. Shatanawi, F. Hasan, T. A. M. Shatnawi, Numerical analysis of Darcy resistant Sutterby nanofluid flow with effect of radiation and chemical reaction over stretching cylinder: induced magnetic field, *AIMS Math.*, **8** (2023), 11202–11220. http://dx.doi.org/10.3934/math.2023567
13. M. A. S. Murad, F. K. Hamasalh, H. F. Ismael, Numerical study of stagnation point flow of Casson-Carreau fluid over a continuous moving sheet, *AIMS Math.*, **8** (2023), 7005–7020. http://dx.doi.org/10.3934/math.2023353
14. K. S. Nisar, M. Shoaib, M. A. Z. Raja, Y. Tariq, A. Rafiq, Design of neural networks for second-order velocity slip of nanofluid flow in the presence of activation energy, *AIMS Math.*, **8** (2023), 6255–6277. http://dx.doi.org/10.3934/math.2023316
15. F. Alsharari, M. M. Mousa, New application of MOL-PACT for simulating buoyancy convection of a copper-water nanofluid in a square enclosure containing an insulated obstacle, *AIMS Math.*, **7** (2022), 20292–20312. http://dx.doi.org/10.3934/math.20221111
16. Z. Mahmood, U. Khan, Nanoparticles aggregation effects on unsteady stagnation point flow of hydrogen oxide-based nanofluids, *Eur. Phys. J. Plus*, **137** (2022), 750. http://dx.doi.org/10.1140/epjp/s13360-022-02917-y
17. K. Guedri, Z. Mahmood, B. M. Fadhl, B. Makhdoum, S. M. Eldin, U. Khan, Mathematical analysis of nonlinear thermal radiation and nanoparticle aggregation on unsteady MHD flow of micropolar nanofluid over shrinking sheet, *Heliyon*, **9** (2023), e14248. http://dx.doi.org/10.1016/j.heliyon.2023.e14248
18. A. Alhowaity, M. Bilal, H. Hamam, M. M. Alqarni, K. Mukdasai, A. Ali, Non-Fourier energy transmission in power-law hybrid nanofluid flow over a moving sheet, *Sci. Rep.*, **12** (2022), 10406. http://dx.doi.org/10.1038/s41598-022-14720-x
19. Adnan, W. Abbas, M. Z. Bani-Fwaz, K. K. Asogwa, Thermal efficiency of radiated tetra-hybrid nanofluid $[(Al_2O_3\text{-}CuO\text{-}TiO_2\text{-}Ag)/water]_{tetra}$ under permeability effects over vertically aligned cylinder subject to magnetic field and combined convection, *Sci. Progress*, **106** (2023), 00368504221149797. http://dx.doi.org/10.1177/00368504221149797
20. K. A. M. Alharbi, Adnan, Thermal investigation and physiochemical interaction of H_2O and $C_2H_6O_2$ saturated by Al_2O_3 and γAl_2O_3 nanomaterials, *J. Appl. Biomater. Func.*, **20** (2022), 22808000221136483. http://dx.doi.org/10.1177/22808000221136483
21. M. Bilal, A. Ali, H. A. Hejazi, S. R. Mahmuod, Numerical study of an electrically conducting hybrid nanofluid over a linearly extended sheet, *J. Appl. Math. Mec.*, **2022** (2022), e202200227. http://dx.doi.org/10.1002/zamm.202200227
22. I. Haq, M. Bilal, N. A. Ahammad, M. E. Ghoneim, A. Ali, W. Weera, Mixed convection nanofluid flow with heat source and chemical reaction over an inclined irregular surface, *ACS Omega*, **7** (2022), 30477–30485. http://dx.doi.org/10.1021/acsomega.2c03919
23. Adnan, M. M. AlBaidani, N. K. Mishra, M. M. Alam, S. M. Eldin, A. A. A. Zahrani, et al., Numerical analysis of magneto-radiated annular fin natural-convective heat transfer performance using advanced ternary nanofluid considering shape factors with heating source, *Case Stud. Therm. Eng.*, **44** (2023), 102825. http://dx.doi.org/10.1016/j.csite.2023.102825

24. A. M. Alqahtani, M. Bilal, M. Usman, T. R. Alsenani, A. Ali, S. R. Mahmuod, Heat and mass transfer through MHD Darcy Forchheimer Casson hybrid nanofluid flow across an exponential stretching sheet, *ZAMM J. Appl. Math. Mec.*, **2023** (2023), e202200213. http://dx.doi.org/10.1002/zamm.202200213
25. K. A. M. Alharbi, Adnan, A. M. Galal, Novel magneto-radiative thermal featuring in SWCNT–MWCNT/$C_2H_6O_2$-H_2O under hydrogen bonding, *Int. J. Mod. Phys. B*, **2023** (2023), 2450017. http://dx.doi.org/10.1142/S0217979224500176
26. Adnan, W. Ashraf, Numerical thermal featuring in γAl_2O_3-$C_2H_6O_2$ nanofluid under the influence of thermal radiation and convective heat condition by inducing novel effects of effective Prandtl number model (EPNM), *Adv. Mech. Eng.*, **14** (2022), 1–11. http://dx.doi.org/10.1177/16878132221106577
27. M. M. Klazly, G. Bognar, Comparison of Sakiadis and Blasius flows using computational fluid dynamic, In: *Solutions for sustainable development*, Boca Raton: CRC Press, 2019. http://dx.doi.org/10.1201/9780367824037-18
28. N. S. Kumar, B. R. Kumar, Blasius and Sakiadis unsteady flow of chemically reacted MHD Williamson fluid with variable conductivity: A comparative study, In: *Advances in fluid dynamics*, 2021. http://dx.doi.org/10.1007/978-981-15-4308-1_67
29. R. L. V. R. Devi, S. V. S. R. Raju, C. S. K. Raju, S. A. Shehzad, F. M. Abbasi, Hydromagnetic Blasius-Sakiadis flows with variable features and nonlinear chemical reaction, *Sci. Iran.*, **28** (2021), 3246–3258. http://dx.doi.org/10.24200/SCI.2021.54288.3681
30. A. Pantokratoras, Blasius and Sakiadis flow with suction and non-linear Rosseland thermal radiation, *Int. J. Thermofluids*, **10** (2021), 100067. http://dx.doi.org/10.1016/j.ijft.2021.100067
31. A. Pantokratoras, Non-similar Blasius and Sakiadis flow of a non-Newtonian Carreau fluid, *J. Taiwan Inst. Chem. E.*, **56** (2015), 1–5. http://dx.doi.org/10.1016/j.jtice.2015.03.021
32. R. C. Bataller, Radiation effects for the Blasius and Sakiadis flows with a convective surface boundary condition, *Appl. Math. Comput.*, **206** (2008), 832–840. http://dx.doi.org/10.1016/j.amc.2008.10.001
33. F. M. Hady, M. R. Eid, M. R. A. Elsalam, M. A. Ahmed, The Blasius and Sakiadis flow in a nanofluid through a porous medium in the presence of thermal radiation under a convective surface boundary condition, *IJEIT*, **3** (2013), 225–234.
34. L. Ali, X. Liu, B. Ali, S. Abdal, R. M. Zulqarnain, Finite element analysis of unsteady MHD Blasius and Sakiadis flow with radiation and thermal convection using Cattaneo-Christov heat flux model, *Phys. Scr.*, **96** (2021), 125219. http://dx.doi.org/10.1088/1402-4896/ac25a3
35. C. M. Krishna, G. V. Reddy, B. Souayeh, C. S. K. Raju, M. R. Gorji, S. S. K. Raju, Thermal convection of MHD Blasius and Sakiadis flow with thermal convective conditions and variable properties, *Microsyst. Technol.*, **25** (2019), 3735–3746. http://dx.doi.org/10.1007/s00542-019-04353-y
36. K. R. Sekhar, G. V. Reddy, C. S. K. Raju, Blasius and Sakiadis flow of magnetohydrodynamic Maxwell fluid with exponentially decaying heat source or sink, *IJRISE*, **2017** (2017), 126–136.
37. A. Pantokratoras, T. Fang, A note on the Blasius and Sakiadis flow of a non-Newtonian power-law fluid in a constant transverse magnetic field, *Acta Mech.*, **218** (2011), 187–194. http://dx.doi.org/10.1007/s00707-010-0406-6

38. F. I. Alao, A. J. Omowaye, A. I. Fagbade, B. Ajayi, Optimal homotopy analysis of Blasius and Sakiadis Newtonian flows over a vertical convective porous surface, *JERA*, **28** (2017), 102–117. http://dx.doi.org/10.4028/www.scientific.net/JERA.28.102
39. A. O. Oyem, W. N. Mutuku, A. S. Oke, Variability effects on magnetohydrodynamic for Blasius and Sakiadis flows in the presence of Dufour and Soret about a flat plate, *Eng. Rep.*, **2** (2020), e12249. http://dx.doi.org/10.1002/eng2.12249
40. A. Pantokratoras, The Blasius and Sakiadis flow along a Riga-plate, *Prog. Comput. Fluid Dy.*, **11** (2011), 329–333. http://dx.doi.org/10.1504/PCFD.2011.042184
41. S. Nadeem, S. Ahmad, N. Muhammad, Computational study of Falkner-Skan problem for a static and moving wedge, *Sens. Actuators B Chem.*, **263** (2018), 69–76. http://dx.doi.org/10.1016/j.snb.2018.02.039
42. Adnan, Heat transfer inspection in $[(ZnO\text{-}MWCNTs)/water\text{-}EG(50:50)]_{hnf}$ with thermal radiation ray and convective condition over a Riga surface, *Wave. Random Complex*, **2022** (2022), 1–15. http://dx.doi.org/10.1080/17455030.2022.2119300
43. Adnan, K. A. M. Alharbi, W. Ashraf, S. M. Eldin, M. F. Yassen, W. Jamshed, Applied heat transfer modeling in conventional hybrid $(Al_2O_3\text{-}CuO)/C_2H_6O_2$ and modified-hybrid nanofluids $(Al_2O_3\text{-}CuO\text{-}Fe_3O_4)/C_2H_6O_2$ between slippery channel by using least square method (LSM), *AIMS Math.*, **8** (2023), 4321–4341. http://dx.doi.org/10.3934/math.2023215
44. Adnan, A. Waqas, Thermal efficiency in hybrid $(Al_2O_3\text{-}CuO/H_2O)$ and ternary hybrid nanofluids $(Al_2O_3\text{-}CuO\text{-}Cu/H_2O)$ by considering the novel effects of imposed magnetic field and convective heat condition, *Wave. Random Complex*, **2022** (2022), 1–16. http://dx.doi.org/10.1080/17455030.2022.2092233
45. Adnan, W. Ashraf, A. H. Alghtani, I. Khan, M. Andualem, Thermal transport in radiative nanofluids by considering the influence of convective heat condition, *J. Nanomater.*, **2022** (2022), 1854381. http://dx.doi.org/10.1155/2022/1854381
46. Adnan, W. Ashraf, I. Khan, M. A. Shemseldin, A. A. A. Mousa, Numerical energy storage efficiency of MWCNTs-propylene glycol by inducing thermal radiations and combined convection effects in the constitutive model, *Front. Chem.*, **10** (2022), 879276. http://dx.doi.org/10.3389/fchem.2022.879276
47. N. Ahmed, Adnan, U. Khan, S. T. Mohyud-Din, I. Khan, R. Murtaza, et al., A novel investigation and hidden effects of MHD and thermal radiations in viscous dissipative nanofluid flow models, *Front. Phys.*, **8** (2020), 75. http://dx.doi.org/10.3389/fphy.2020.00075
48. T. Watanabe, Thermal boundary layers over a wedge with uniform suction or injection in forced flow, *Acta Mech.*, **83** (1990), 119–126. http://dx.doi.org/10.1007/BF01172973
49. Adnan, R. Murtaza, I. Hussain, Z. Rehman, I. Khan, M. Andualem, Thermal enhancement in Falkner-Skan flow of the nanofluid by considering molecular diameter and freezing temperature, *Sci. Rep.*, **12** (2022), 9415. http://dx.doi.org/10.1038/s41598-022-13423-7

AIMS Press